balt4/pq-pnas/pq-pnas/pq-orig/pq0900d03a | dumhartm | S=7 | 6/11/03 | 16:22 | 4/Color Figure(s): 1-3 | Art: 03-0900 | Input-as

Complex landscape of protein structural dynamics unveiled by nanosecond Laue crystallography

Dominique Bourgeois[†‡§¶], Beatrice Vallone[§‖], Friedrich Schotte[††], Alessandro Arcovito[‖], Adriana E. Miele[‖], Giuliano Sciara[‖], Michael Wulff[‡], Philip Anfinrud[††], and Maurizio Brunori[‖]

[†]Laboratoire de Cristallographie et de Cristallogénèse des Protéines, Unité Mixte de Recherche 9015, Institut de Biologie Structurale/Commissariat à l'Energie Atomique/Université Joseph Fourier, 41 rue Jules Horowitz, 38027 Grenoble Cedex 1, France; [‡]European Synchrotron Radiation Facility, 6 rue Jules Horowitz, BP 220, 38043 Grenoble Cedex, France; [‖]Dipartimento Scienze Biochimiche and Istituto Pasteur-Fondazione Cenci Bolognetti, Università di Roma ''La Sapienza'', Piazzale A. Moro 5, 00185 Rome, Italy; and [††]Laboratory of Chemical Physics, National Institute of Diabetes and Digestive and Kidney Diseases, National Institutes of Health, Bethesda, MD 20892-0520

Edited by Robert H. Austin, Princeton University, Princeton, NJ, and approved May 19, 2003 (received for review February 14, 2003)

AQ: A

Although conformational changes are essential for the function of proteins, little is known about their structural dynamics at atomic level resolution. Myoglobin (Mb) is the paradigm to investigate conformational dynamics because it is a simple globular heme protein displaying a photosensitivity of the iron–ligand bond. Upon laser photodissociation of carboxymyoglobin Mb a nonequilibrium population of protein structures is generated that relaxes over a broad time range extending from picoseconds to milliseconds. This process is associated with migration of the ligand to cavities in the matrix and with a reduction in the geminate rebinding rate by several orders of magnitude. Here we report nanosecond time-resolved Laue diffraction data to 1.55-Å resolution on a Mb mutant, which depicts the sequence of structural events associated with this extended relaxation. Motions of the distal E-helix, including the mutated residue Gln-64(E7), and of the CD-turn are found to lag significantly (100–300 ns) behind local rearrangements around the heme such as heme tilting, iron motion out of the heme plane, and swinging of the mutated residue Tyr-29(B10), all of which occur promptly (≤3 ns). Over the same delayed time range, CO is observed to migrate from a cavity distal to the heme known to bind xenon (called Xe4) to another such cavity proximal to the heme (Xe1). We propose that the extended relaxation of the globin moiety reflects reequilibration among conformational substates known to play an essential role in controlling protein function.

myoglobin | protein dynamics | conformational states | functional intermediates | protein crystallography

Fn1

Conformational relaxations in proteins are characterized by a unique and very complex time-dependant structure. In myoglobin (Mb), reequilibration between conformational substates extends over at least six orders of magnitude in time, from picoseconds to nanoseconds (1). In parallel, functional properties respond with a drop in ligand binding reactivity of >1,000-fold, as established by transient laser spectroscopy (2, 3). This is the manifestation of the existence and the role of a myriad of conformational substates that interconnect over the complex and rugged energy landscape of a protein (4, 5). Internal fluctuations are thought to permit interchange between conformational substates, thereby accounting for variations in substrate accessibility to the active site, ligand migration through the protein matrix, and ligand recombination after transient trapping within the protein. The structural basis of this extended conformational relaxation is, however, still largely unknown. We report an experiment by time-resolved Laue crystallography that unveils aspects of the complex time dependence of the structure of Mb and shows unexpected structural dynamics associated with the extended relaxation of the protein as observed in a large ensemble of molecules.

Investigations of internal fluctuations have often been carried out on heme proteins, because of the possibility to rapidly photodissociate ligands such as O_2, CO, or NO bound to ferrous heme iron (6), allowing synchronous initiation of the reaction and observation of ligand migration and globin relaxation in a large assembly of molecules. Outstanding progress has been achieved in the past through analysis of transients by kinetic methods based on a variety of spectroscopic probes and laser pump pulses from femtoseconds to nanoseconds (2, 3, 7, 8). However, spectroscopy does not provide direct information on the global conformational changes of the protein moiety that are involved in the control of overall reaction rates. Being a relatively simple and well characterized protein with excellent diffraction power, crystalline carboxymyoglobin (MbCO) has become therefore the paradigm to attack the problem of structural dynamics by x-ray crystallography. This approach started with low (or ultralow) temperature investigations of the photoproduct, which allowed the trapping of early intermediates along the globin relaxation pathway (refs. 9 and 10 and references therein). In pioneering time-resolved Laue diffraction studies of photolyzed wild-type MbCO, at room temperature, Moffat and coworkers (11, 12) observed at ≈1.8-Å resolution structural changes whose time dependence revealed the migration of CO from a primary to a secondary docking site before rebinding. The secondary docking site, proximal to the heme and called the Xe1 site, is one of four hydrophobic cavities in Mb known to host xenon (13). That CO becomes transiently trapped in this site at physiological temperatures provides direct confirmation for the functional relevance of such cavities (8, 14, 15) and raises the significance of studies in which similar states were characterized by low-temperature crystallography (refs. 10 and 16 and references therein). However, time-dependent changes of the globin conformation remained largely unresolved (12), frustrating attempts to unveil the structural basis of the extended conformational relaxation governing ligand migration through the matrix.

Substantial improvements in Laue diffraction methodology (17), combined with outstanding protein crystal quality, allowed us to obtain nanosecond time-resolved diffraction data to 1.55-Å resolution, at a level of detail sufficient to assess the structural origins of the extended conformational relaxation in proteins. We used a triple mutant of sperm whale Mb, denoted YQR-Mb [Leu29(B10)Tyr, His64(E7)Gln, Thr67(E10)Arg], which was originally engineered to mimic the hemoglobin of pig roundworm *Ascaris suum* (18). Ligand binding to this mutant is slower than to wild-type Mb by approximately one order of magnitude, thereby extending the window of time over which conforma-

AQ: B

BIOPHYSICS

This paper was submitted directly (Track II) to the PNAS office.

Abbreviations: Mb, myoglobin; MbCO, carboxymyoglobin; YQR-Mb, Mb triple mutant [Leu29(B10)Tyr, His64(E7)Gln, Thr67(E10)Arg].

Data deposition: The crystallographic coordinates and observed structure factor amplitudes have been deposited in the Protein Data Bank, www.rcsb.org (PDB ID codes 1MYZ for YQR-MbCO and 1MZ0 for YQR-Mb*).

[§]D.B. and B.V. contributed equally to this work.

[¶]To whom correspondence should be addressed. E-mail: bourgeoi@lccp.ibs.fr.

Cadmus: 1853

Table 1. Diffraction data

	Data set					
	Dark*	3 ns	32 ns	316 ns†	3.16 μs	3 ms
Resolution, Å	1.55	1.55	1.55	1.55	1.55	1.55
No. of observations	832,442	79,843	73,036	79,853	77,004	71,274
No. of unique reflections‡	31,195	24,800	24,818	25,942	25,041	23,717
Completeness, %‡	96.0	77.4	78.9	80.1	79.7	91.8
∞–2.0 Å	99.5	92.9	94.9	94.7	94.7	91.8
Outer shell§	75.9	35.3	38.7	37.7	42.3	28.5
R_{sym}, %¶	6.4	6.7	5.5	5.9	5.9	7.3
Outer shell§	41.4	17.0	19.5	17.3	18.5	19.6
Mean $I/\sigma(I)$	37.1	12.2	12.9	13.0	12.6	10.7
Outer shell§	4.5	3.2	2.7	3.3	2.1	3.1
Laser energy, mJ	—	5.7	5.0	4.7	5.0	6.5
Photolysis level, %	—	20.5	21.4	18.4	22.0	24.6

*Merge of 10 individual data sets.
†This data set was used in the refinement.
‡The space group is *P*6.
§Outer shell was 1.62–1.55 Å. R_{merge} on the intensities between the dark state and the five excited states were 9.0%, 10.1%, 8.2%, 9.7%, and 9.3%, respectively.
¶$R_{sym} = \Sigma_j\Sigma_h|Ih, j - \langle Ih\rangle|/\Sigma_j\Sigma_h Ih, j$.

tional changes can be monitored. We provide evidence that a significant fraction of the photodissociated CO first reaches a cavity on the distal side of the heme (19) on the nanosecond time scale and then migrates to a cavity on the proximal side of the heme on the 100–300-ns time scale, in agreement with Srajer *et al.* (12). Of more general significance, the relaxation of the globin toward a deoxy-like conformation clearly lags behind CO photodissociation and heme relaxation, showing an extended time course of the internal motions. These observations are consistent with a reequilibration among conformational substates as expected from the complex energy landscape of a protein (5) and with models proposed to account for the correlations between ligand binding and conformational relaxation in Mb (3, 20, 21), conferring general significance to our results.

AQ: C

Materials and Methods

Protein Crystals. Mutant YQR-Mb was produced in *Escherichia coli* starting from a synthetic gene also containing the substitution Asp122Asn. This additional conservative mutation shows negligible functional and structural variations with respect to wild-type Mb and crystallizes in space group *P*6 (22). Seeded batch crystallization of *P*6 YQR-MbCO was accomplished in vials stored at 294 K within a gas-tight vessel periodically purged with CO. YQR-MbCO crystals arose within 1 week from the growth medium (CO-saturated, pH 8.7, 2.8 M ammonium sulfate/100 mM Tris-Cl/1 mM dithionite). Optimal sized crystals (200 to 300-μm diameter hexagonal rods) were mounted in CO-purged capillaries (fused silica, 1-mm diameter). Mineral oil plugs were inserted on either side of the crystal to minimize thermal-induced distillation of solvent to/from the mother liquor surrounding the protein.

Laser Photolysis. Mb crystals were photolyzed with 630-nm, 2.2-ns (full width at half maximum), circularly polarized laser pulses generated by a Nd:YAG-pumped optical parametric oscillator (Opotek Vibrant, Quantel, Santa Clara, CA). The laser beam propagated parallel to the goniometer rotation axis and perpendicular to the x-ray beam. The capillary was oriented at 45° relative to the goniometer axis to illuminate the same hexagonal face of the crystal at any spindle position. Photolysis energies were limited to 4–5 mJ/mm^2 to avoid pump-induced streaking of the diffraction spots. A 4-mJ/mm^2 630-nm pulse incident on a 200-μm thick crystal delivers ≈3.5 incident photons per heme, about half of which are absorbed, thereby causing a temperature increase of about 2°C. To extract the excess heat, the capillary was bathed in a ≈10°C gas stream (Oxford Cryosystem 600). The achieved level of photolysis was constrained by a possible ultrafast geminate recombination and by the presence of a residual amount (<10%) of oxidized met-Mb displaying high optical density at 630 nm.

AQ: D

Laue Data Collection. Laue diffraction data (23) were acquired on the ID09B beamline at the European Synchrotron Radiation Facility (ESRF, Grenoble, France). With the synchrotron operated in single bunch mode, a narrow-band undulator generated ≈150-ps x-ray pulses containing 2×10^9 photons per pulse in a relative bandwidth of 6% full width at half maximum peaked at 0.75 Å (17, 24). Each time-resolved diffraction data set comprised 31 still images collected at equally spaced angular settings spanning 60°. To improve the signal-to-noise ratio, each image was averaged over 64 pump-probe measurements accumulated at 3 Hz on a Mar charg-coupled device detector. To minimize radiation damage and progressive oxidation to met-Mb, a fresh crystal was used for each pump-probe time delay (3.2 ns, 32 ns, 316 ns, 3.16 μs, and 3 ms). To scale the level of photolysis from crystal to crystal, a data set at a common time point (32 ns) was collected for each crystal. In addition, a "dark" (nonphotolyzed) data set was collected. The time delay between the laser and x-ray pulses was set to a precision of <0.5 ns with a computer-controlled digital delay generator (Stanford Research Systems DG535, Sunnyvale, CA).

AQ: E

Data Processing. Laue diffraction data were reduced in a fully automated way (24) by using LAUEGEN, PROW, and LSCALE (Table 1). A YQR-MbCO dark-state model was refined by using CNS (25) and O (26) for model building, from data obtained by merging 10 dark data sets (Table 2), and by using as a starting structure a low-temperature model of YQR-MbCO without water molecules. Electron density difference maps ($F_{light} - F_{dark}$) were generated with CCP4 (27) by using phases from this dark-state model, after optimization with a Bayesian statistics-based method (28). The initial model for the photoexcited YQR-Mb*, refined against the 316-ns data set, contained two conformations: the dark state (conformer 1) and the same state with bound CO removed and free CO added at the Xe1 site

T1 T2 AQ: F

Table 2. Refinement statistics and geometry

	Data set	
	Dark	Light (316 ns)
Refinement		
No. of refined residues	153	153
No. of residues with dual conformations	12	0
Total no. of water molecules	145	145
R_{cryst}, %†	16.6	15.0
R_{free}, %†‡	18.4	17.4
Rmsd on bond lengths, Å	0.0043	0.009
Rmsd on bond angles, °	1.03	1.43
Rmsd coordinate error, Å§	0.11	0.09¶
Average *B* factor, Å^2	19.4	20.3
Light state occupancy, %	—	18
Geometry		
Iron displacement, Å	—	0.27
Heme tilt,‖ °	—	5.58
E-helix mean displacement, Å**	—	0.56
F-helix mean displacement, Å	—	0.23
CD-turn mean displacement, Å	—	0.69
Rmsd to YQR-Mb deoxy state, Å	0.248	0.167

Rmsd, root-mean-square deviation.
*$R_{cryst} = \Sigma_h ||F_{obs}(h)| - |F_{calc}(h)|| / \Sigma_h |F_{obs}(h)|$.
†Used resolution range: 500–1.6 Å.
‡Calculated with 5% randomly selected reflections excluded.
§As estimated by a σ_A plot (29).
¶Corresponds to the mixture of the dark and light states.
‖Angle between the planes defined by atoms C4B, C1D, C3C of the heme.
**Taken over residues 59–68.

(conformer 2). The initial occupancy of conformer 2 was set to the photolysis yield (≈18%) as estimated by integration of the negative electron density feature at the bound CO position and comparison with simulated data of equal completeness. Stereochemical parameters for the heme geometry were relaxed to allow heme bending and out-of-plane displacement of the iron. Conformer 2 was subjected to conjugate gradient minimization and *B*-factor refinement while conformer 1 was held in place. Manual rebuilding was performed where residual ($F_{light} - F_{calc}$) electron density superimposed to ($F_{light} - F_{dark}$) density. The overall occupancy of the two conformers was then refined and the whole procedure was repeated until convergence (29). Reliable refinement of more than two conformers would be needed to model accurately the time-dependant changes observed in ($F_{light} - F_{dark}$) difference maps. With the available data, attempts to perform such refinement with common procedures were unsuccessful. Figs. 1 and 2 were drawn by using BOBSCRIPT (30) and RASTER3D (31). Difference ($F_{light} - F_{dark}$) maps were integrated above/below $\pm 3.5\sigma$ with a homemade routine based on a connectivity search algorithm. Scaling between crystals to account for variations in photolysis yield was performed by normalization of the total integrated positive difference density $>3.0\ \sigma$ for all 32-ns data sets.

AQ: G

Results and Discussion

Fig. 1 depicts the structural changes observed 316 ns after laser photolysis of YQR-MbCO, which were confirmed by refinement of a model of YQR-Mb*, closely resembling the deoxy state (Table 2). The most pronounced structural changes appear on the distal side of the heme and involve: (*i*) disappearance of the bound CO; (*ii*) displacement of the iron out of the heme plane toward the proximal His-93(F8); (*iii*) tilt and translation of the heme; (*iv*) motion of Tyr-29(B10) toward the space vacated by photodissociated CO; (*v*) displacement of the E-helix with major structural changes occurring at and near Gln-64(E7); and (*vi*) displacement of the CD-turn with an upward motion of Phe-43(CD1) and a large rotation of Phe-46(CD4). Although motions on the proximal side are less pronounced compared with wild-type Mb (12), a positive density modeled with CO (partial occupancy) is observed in the Xe1 docking site, a cavity circumscribed by Leu-89(F4), Ile-101(G2), Leu-104(G5), and Phe-138(H15) (13). F1

The time evolution of the photolysis-induced structural differences is depicted in Fig. 2. Most of the difference electron density in the vicinity of the heme is virtually time invariant from 3 ns onwards, except for the 3-ms time point, indicating that the corresponding structural changes (dissociation of CO, motion of the iron, and tilting of the heme) develop fully by 3 ns and decay in amplitude only as the CO rebinds. The swinging motion of F2

BIOPHYSICS

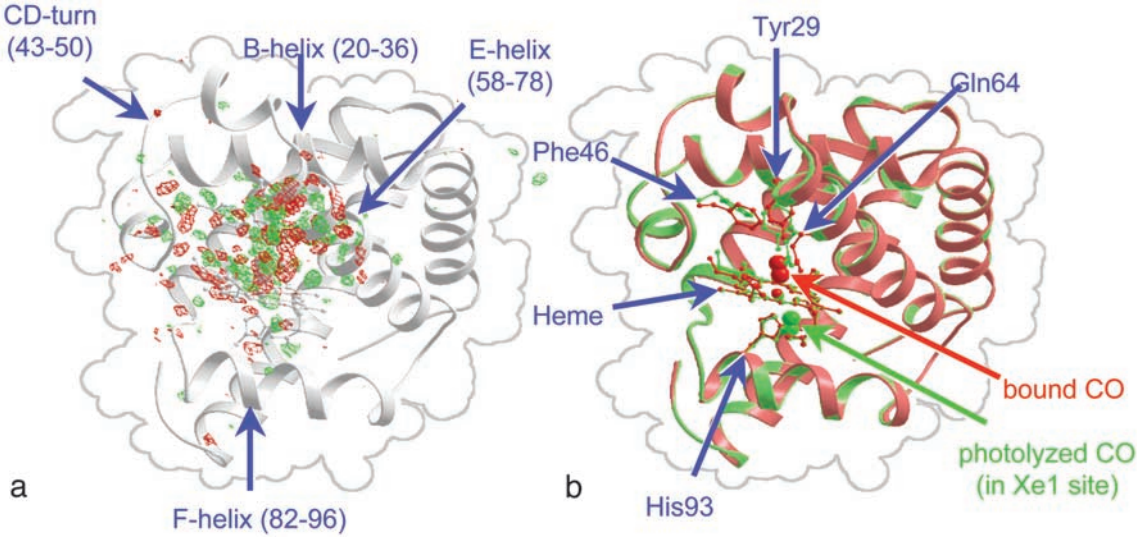

Fig. 1. Structural changes in YQR-Mb 316 ns after photolysis. (*a*) Overlay of ($F_{light} - F_{dark}$) difference electron density maps on the YQR-MbCO model (red, negative; green, positive; contoured at 3.5σ, where σ is the standard deviation of the electron density difference). Most changes are clustered on the distal (upper) side of the heme. (*b*) Overview of the modeled structure of YQR-MbCO (red) and YQR-Mb* (green). The heme and several key residues are rendered as balls and sticks, the CO as space filling, and the rest of the protein as ribbon.

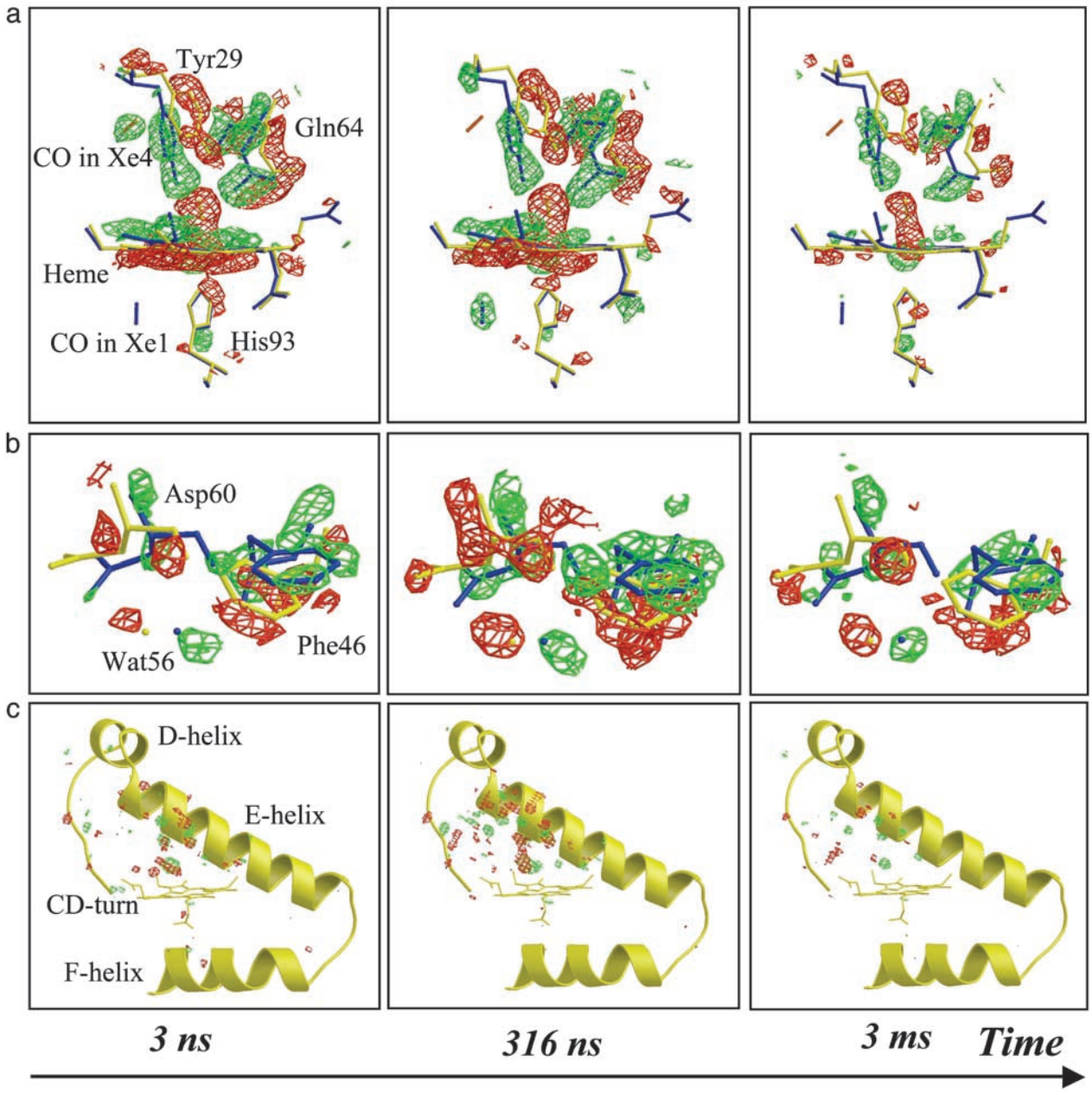

Fig. 2. Detailed view of the time-dependent electron density differences (red, negative; green, positive) overlaid on the models of YQR-MbCO (yellow) and YQR-Mb* (blue). (*a*) Heme vicinity: the disappearance of bound CO, tilting of the heme, swinging motion of Tyr-29(B10), and migration of photolyzed CO to the Xe4 docking site (shown in orange) are fully developed by 3 ns (contoured to 3.0σ); by 316 ns, the photolyzed CO has reached the Xe4 docking site. (*b*) Concerted motion of Asp-60(E3), Phe-46(CD4), and Wat56, reaching a maximum amplitude by 316 ns (contoured to 3.0σ). (*c*) Overview of structural changes taking place around the E-helix, CD-turn, and F-helix (contoured to 4.0σ).

Tyr-29(B10) also occurs before 3 ns, making this residue the fastest globin sensor of CO release. Solution-phase time-resolved near-infrared spectroscopy on wild-type Mb (1) revealed that the conformational relaxation extends from ≈10 ps to almost 1 μs with a stretched time course. We believe that the major fraction of the optical change, occurring below 1 ns (1), may well reflect the prompt local motions observed in the vicinity of the heme, in agreement with studies by temperature-derivative infrared spectroscopy on the YQR and other Mb mutants (20, 21).

AQ: H

In contrast, the difference electron density about Gln-64(E7), Asp-60(E3), and Phe-46(CD4) continues to develop from 3 ns to 316 ns, similar to the electron density covering the entire E-helix and CD-turn, as quantified in Fig. 3. Evidently, a few hundred nanoseconds is required for the globin to fully respond to the prompt structural changes of the heme and Tyr-29(B10). Remarkably, motion of Gln-64(E7) appears to be slaved to that of the E-helix, which has a nearly identical time course. Thus, the return motion of Tyr-29(B10) and Gln-64(E7), required for ligand recombination, is expected to be damped by motion of the E-helix, thereby providing an additional enthalpy barrier contributing to the slow recombination rate characteristic of YQR-Mb (18). The synchrony between motions of the E-helix and the CD-turn appears to be promoted by a mutual steric hindrance between Asp-60(E3) and Phe-46(CD4). In addition, the concerted large-scale motions of these two secondary struc-

F3

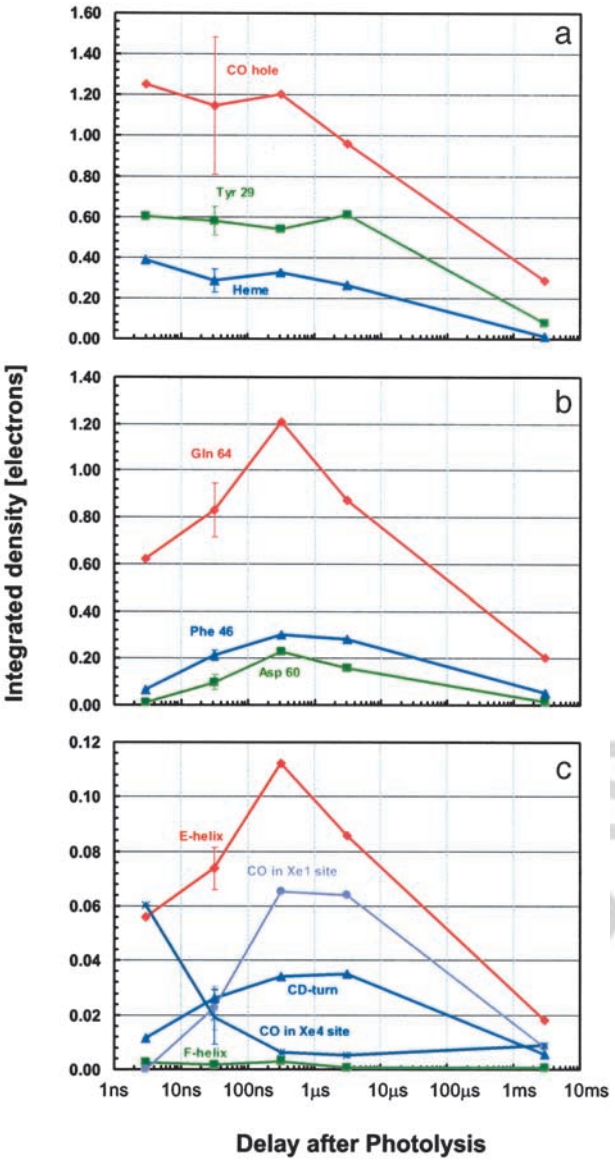

Fig. 3. Time dependence of difference electron density for key structural features. The numerical values reflect the integral of the positive electron density beyond 3.5σ (negative density for CO hole) corrected for variations in photolysis yield. The error bars at 32-ns delay correspond to twice the rms deviation among the four data sets collected at this delay. (*a*) Key features that appear promptly. (*b*) Key residues whose displacement attains a maximum amplitude at around 316 ns. (*c*) Secondary structures whose overall displacement also attains a maximum amplitude at around 316 ns. The average integrated density per residue is shown; the occupation by CO of the Xe4 and Xe1 docking sites is also reported by displaying the total integrated density divided by 10 for scaling purposes.

ture elements are probably coupled because the formation of the CO hole triggers the swinging motion of Gln-64(E7) while the synchronous heme tilt initiates an up-kick of the Phe-43(CD1) aromatic ring, which propagates upwards. Interestingly, the structural perturbation on the proximal His-93(F8), caused by the iron–heme displacement, appears to have a negligible effect on the F-helix (Fig. 3*c*). The time lag of the large-scale motions observed here suggests that these motions may be slaved to fluctuations of the solvent (32).

The rapid rearrangement of Tyr-29(B10) (Fig. 3*a*) seems not to be coupled to, and may in fact follow, migration of photolyzed CO to the Xe4 binding site distal to the heme (13), already observed by ultralow-temperature crystallography (19). Indeed, when YQR-MbCO is photolyzed at 30 K, Tyr-29(B10) cannot relax and stays put, although the Xe4 cavity is found to host CO. Analysis of difference electron densities shows that at room temperature CO propagates beyond Xe4 and populates the Xe1 cavity proximal to the heme (Fig. 2*a*), reaching maximum occupancy ≈300 ns after photolysis and then decaying with a time course consistent with either rebinding or diffusion into the bulk (Fig. 3*c*). The synchrony between large-scale motions of the globin and occupation of the Xe1 site by CO is consistent with low-temperature studies showing that migration to this site does not occur below the temperature of the dynamical transition, where anharmonic motions of the protein are quenched (16, 20, 21, 33). The system of cavities shown to host photodissociated CO (10, 14, 15) is contiguous in space; in fact, the Xe2 site bridges Xe4 and Xe1 via, respectively, Ile-107(G8) and Leu-104(G5). Interestingly, we observe a displacement (0.4 Å) of Leu-104(G5) Cδ while CO populates the Xe1 site (not shown), suggesting a gating mechanism for internal migration.

Concluding Remarks

Our observation of asynchronous internal motions of different parts of the globin moiety may be taken as clear-cut structural evidence for the stretched-time course of deoxy-Mb relaxation (1) and the complex energy surface of a protein (5). The extended dynamics of the internal motions in YQR-Mb seems to support the idea that the protein populates different conformational substates (4), and that internal motions occur at different rates. We envisage that we have observed the conformational relaxation of the globin, which begins in the picosecond time regime with bending of the heme but extends over several orders of magnitude in time, in agreement with expectations from time-resolved spectroscopy (1, 3). The physical basis of this extended and complex time dependence of the structure of internal motions is as yet uncertain, but it is tempting to correlate our observation with previous investigations (3, 16, 20, 21, 32, 34) on the effect of temperature and solvent viscosity on the conformational relaxation kinetics of Mb. Accordingly, it may be assumed that the heterogeneous nature of the protein core is associated with a complex and heterogeneous friction of the protein interior, leading to an extended time dependence of the internal conformational changes. Because crystallography yields information on the mean structure of all units in the crystal, it is likely that the delayed structural changes arise from evolution in the relative occupancies of a spatial juxtaposition of conformational substates. Therefore, our data support the hypothesis that the stretched relaxation involves a reequilibration between these conformational substates. In summary, our results shed light on the general significance of the hierarchical nature of the energy landscape of a protein (5) and also demonstrate the power of time-resolved Laue crystallography studies at room temperature to observe directly the dynamics of protein conformational changes.

This article is dedicated to Eraldo Antonini on the occasion of the 20th anniversary of his untimely death on March 19, 1983. We thank William A. Eaton (Bethesda, MD) for fruitful discussions and Keith Moffat (Chicago, IL) for his pioneering contributions to the field of time-resolved crystallography. Support from the Ministry of Research of Italy ("Structural dynamics of heme proteins") is acknowledged.

1. Jackson, T. A., Lim, M. & Anfinrud, P. A. (1994) *Chem. Phys.* **180,** 131–140.
2. Steinbach, P. J., Ansari, A., Berendsen, J., Braunstein, D., Chu, K., Cowen, B. R., Ehrenstein, D., Frauenfelder H., Johnson, J. B. & Lamb, D. C. (1991) *Biochemistry* **30,** 3988–4001.
3. Ansari, A., Jones, C. M., Henry, E. R., Hofrichter, J. & Eaton, W. A. (1994) *Biochemistry* **33,** 5128–5145.
4. Austin, R. H., Beeson, K. W., Eisenstein, L., Frauenfelder, H. & Gunsalus, I. C. (1975) *Biochemistry* **14,** 5355–5373.

5. Frauenfelder, H., Sligar, S. G. & Wolynes, P. G. (1991) *Science* **254,** 1598–1603.
6. Gibson, Q. H. (1989) *J. Biol. Chem.* **264,** 20155–20158.
7. Lim, M., Jackson, T. A. & Anfinrud, P. A. (1993) *Proc. Natl. Acad. Sci. USA* **90,** 5801–5804.
8. Scott, E. E. & Gibson, Q. H. (1997) *Biochemistry* **36,** 11909–11917.
9. Schlichting, I., Berendzen, J., Phillips, G. N. & Sweet, R. M. (1994) *Nature* **371,** 808–812.
10. Schlichting, I. & Chu, K. (2000) *Curr. Opin. Struct. Biol.* **10,** 744–752.
11. Srajer, V., Teng, T. Y., Ursby, T., Pradervand, C., Ren, Z., Adachi, S., Schildkamp, W., Bourgeois, D., Wulff, M. & Moffat, K. (1996) *Science* **274,** 1726–1729.
12. Srajer, V., Ren, S., Teng, T., Schmidt, M., Ursby, T., Bourgeois, D., Pradervand, C., Schildkamp, W., Wulff, M. & Moffat, K. (2001) *Biochemistry* **40,** 13802–13815.
13. Tilton, R. F., Kuntz, I. D. & Petsko, G. A. (1984) *Biochemistry* **23,** 2849–2857.
14. Scott, E. E., Gibson, Q. H. & Olson, J. S. (2001) *J. Biol. Chem.* **276,** 5177–5188.
15. Brunori, M. & Gibson, Q. H. (2001) *EMBO Rep.* **2,** 674–679.
16. Ostermann, A., Waschipky, R., Parak, F. G. & Nienhaus, G. U. (2000) *Nature* **404,** 205–208.
17. Schotte, F., Techert, S., Anfinrud, P. A., Srajer, V., Moffat, K. & Wulff, M. (2002) in *Third-Generation Hard X-ray Synchrotron Radiation Sources*, ed. Mills, D. (Wiley, New York), pp. 345–401.
18. Brunori, M., Cutruzzolà, F., Savino, C., Travaglini-Allocatelli, C., Vallone, B. & Gibson, Q. H. (1999) *Biophys. J.* **76,** 1259–1269.
19. Brunori, M., Vallone, B., Cutruzzolà, F., Travaglini-Allocatelli, C., Berendzen, J., Chu, K., Sweet, R. M. & Schlichting, I. (2000) *Proc. Natl. Acad. Sci. USA* **97,** 2058–2063.
20. Lamb, D. C., Nienhaus, K., Arcovito, A., Draghi, F., Miele, A. E., Brunori, M. & Nienhaus, U. (2002) *J. Biol. Chem.* **277,** 11636–11644.
21. Nienhaus, K., Lamb, D. C., Deng, P. & Nienhaus, G. U. (2002) *Biophys J.* **82,** 1059–1067.
22. Phillips, G. N., Arduini, R. M., Springer, B. A. & Sligar, S. G. (1990) *Proteins* **7**, 358–365.
23. Bourgeois, D., Ursby, T., Wulff, M., Pradervand, C., Legrand, A., Schildkamp, W., Labouré, S., Srajer, V., Teng, T. Y., Roth, M. & Moffat, K. (1996) *J. Synchrotron Radiat.* **3,** 65–74.
24. Bourgeois, D., Wagner, U. & Wulff, M. (2000) *Acta Crystallogr. D* **56,** 973–985.
25. Brünger, A. T., Adams, P. D., Clore, G. M., DeLano, W. L., Gros, P., Grosse-Kunstleve, R. W., Jiang, J. S., Kuszewski, J., Nilges, M., Pannu, N. S., *et al.* (1998) *Acta Crystallogr. D* **54,** 905–921.
26. Jones, T. A., Bergdoll, M. & Kjeldgaard, M. (1990) in *Crystallographic and Modelling Methods in Molecular Design*, eds. Bugg, C. & Ealick, S. (Springer, New York), pp. 189–199.
27. Collaborative Computational Project Number 4 (1994) *Acta Crystallogr. D* **50,** 760–763.
28. Ursby, T. & Bourgeois, D. (1997) *Acta Crystallogr. A* **53,** 564–575.
29. Royant, A., Edman, K., Ursby, T., Pebay-Peyroula, E., Landau, E. M. & Neutze, R. (2000) *Nature* **406,** 645–648.
30. Esnouf, R. M. (1997) *J. Mol. Graphics* **15,** 132–134.
31. Merritt, E. A. & Murphy, M. E. P. (1994) *Acta Crystallogr. D* **50,** 869–873.
32. Fenimore, P. W., Frauenfelder, H., McMahon, B. H. & Parak, F. G. (2002) *Proc. Natl. Acad. Sci. USA* **99,** 16047–16051.
33. Chu, K., Vojtchovsky, J., McMahon, B. H., Sweet, R. M., Berendzen, J. & Schlichting, I. (2000) *Nature* **403,** 921–923.
34. Hagen, S. J. & Eaton, W. A. (1996) *J. Chem. Phys.* **104,** 3395–3398.

AQ: I